**Dielectric metasurfaces for complete control of phase, amplitude and polarization**

*Tong Wu, Xueqian Zhang*, Quan Xu, Eric Plum, Kaiji Chen, Yuehong Xu, Yongchang Lu, Huifang Zhang, Ziying Zhang, Xieyu Chen, Guanhua Ren, Li Niu, Zhen Tian, Jiaguang Han* and Weili Zhang**

T. Wu, Dr. X. Zhang, Dr. Q. Xu, K. Chen, Y. Xu, Y. Lu, Z. Zhang, X. Chen, G. Ren, L. Niu, Prof. Z. Tian, Prof. J. Han
Center for Terahertz waves and College of Precision Instrument and Optoelectronics Engineering, Tianjin University and the Key Laboratory of Optoelectronics Information and Technology (Ministry of Education)
Tianjin 300072, People's Republic of China
E-mail: alearn1988@tju.edu.cn; jiaghan@tju.edu.cn

Prof. E. Plum
Optoelectronics Research Centre and Centre for Photonic Metamaterials,
University of Southampton,
Highfield, Southampton SO17 1BJ, UK

Dr. H. Zhang
Cavendish Laboratory
University of Cambridge,
J. J. Thomson Avenue, CB3 OHE Cambridge, United Kingdom

Prof. W. Zhang
School of Electrical and Computer Engineering
Oklahoma State University
Stillwater, Oklahoma 74078, USA
E-mail: weili.zhang@okstate.edu

Keywords: Dielectric metasurface, complete control, interference, meta-hologram, terahertz

**Abstract**

The achievable functionalities of metasurfaces are mainly determined by the capability of the unit cells in controlling the local electromagnetic responses. To realize full control of the light propagation, it is highly desired to find a kind of unit cell that can achieve complete control of the phase, amplitude and polarization, which remains a big challenge and cannot be fully replaced with iteration algorithms. Here, we achieve such control by exploiting interference in a dielectric unit cell composed of multiple meta-atoms, namely, a meta-molecule. This strategy provides more effective geometric degrees of freedom within the meta-molecule, enabling full control over its optical properties, as we demonstrate with a complete meta-molecule database. As a proof-of-concept demonstration, a polarization-independent, a polarization-dependent, and a vectorial meta-hologram are proposed and experimentally characterized. High imaging quality is achieved in both the measured intensity and phase distributions. This is allowed by the ability of our meta-molecules to fully record the information of the target images. Our strategy opens a direct way towards optical devices with various desirable functionalities.

## 1. Introduction

Manipulating light propagation in an arbitrary designable manner is one of the ultimate goals in optics. Metasurfaces, artificial two-dimensional planes consisting of subwavelength meta-atoms, provide a powerful platform for accomplishing this task. [1-3] A variety of devices with diverse functionalities have been demonstrated using metasurfaces, such as beam deflectors, [4-7] meta-lenses,[8-10] special beam generators[11-13] and holograms,[14-17] etc. Generally speaking, the ability of a metasurface to manipulate the wavefront depends on the light-engineering capability of its unit cell, i.e. the simultaneous and independent level of control over the basic electromagnetic scattering parameters that control the electromagnetic field's phase, amplitude, and polarization. Recent advances[18] have also shown that the more parameters the unit cells can control, the more complex functionalities the metasurfaces can realize, such as high-quality and multi-output-channel imaging allowed by phase and amplitude control,[19-21] as well as vectorial field generation allowed by polarization-dependent phase control.[13,22,23] However, these studies are all failing in achieving complete control over these parameters. Thus, the functionalities are limited to a single polarization working channel or certain types of polarization distributions, for example, spatially symmetric polarization distributions. Though applying iterative algorithms can help,[24] they cannot truly remedy the missing degree(s) of freedom, resulting in inevitable background noise. It is highly desirable to develop new unit cell designs that are capable of fully controlling the electromagnetic field.

In general, the number of degrees of freedom of the electromagnetic field that may be independently controlled are implicitly related to the effective geometric freedoms of the unit cell. This relation is true for both dielectric unit cells that rely on Mie and waveguide resonances, and plasmonic unit cells that rely on plasmonic resonances.[25-27] For example, linearly cross-polarized phase control depends on the degree of anisotropy,[4,5] linearly co-polarized phase control on the effective cavity length along the polarization direction,[28,29]

Pancharatnam-Berry phase control on the angle of rotation,[8,30] phase and amplitude/polarization control on the anisotropic and rotational degrees of freedom,[13,22,31,32] phase control for orthogonal linear polarizations on the effective cavity length along the two orthogonally polarized directions,[33,34] etc. The above cases are all based on unit cells consisting of single meta-atoms controlling up to two electromagnetic properties with two effective geometric degrees of freedom. However, four degrees of freedom are needed for achieving complete control, i.e. independent control over phases and amplitudes in two orthogonal polarization channels. Therefore, additional geometric degrees of freedom need to be exploited.

A simple design strategy for addressing the above problem is to introduce another meta-atom into the unit cell design, namely, forming a meta-molecule,[35-37] where the effective geometric freedoms can be doubled. This allows interference of the scattering fields from the two meta-atoms to be exploited to control the electromagnetic field. For example, the amplitude and phase of the overall scattered field can be controlled by solely manipulating the individual phase responses of the two meta-atoms,[38-41] or making the two meta-atoms respectively manipulate the amplitude and the phase in a double layer configuration[42]. Suitable scattering responses of a single meta-atom are actually quite easy to realize by simply tuning its geometric degrees of freedom. By taking advantage of such an effect in two orthogonal polarization channels, simultaneous and independent control over the entire parameter space of amplitude and phase was demonstrated very recently in the visible range. However, either oblique incidence is required,[43] or the effective size of the meta-molecules is larger than the working wavelength,[44] which may introduce unwanted diffraction losses.

In this work, we propose a general subwavelength meta-molecule design that allows complete control over the entire parameter space of transmission phases and amplitudes of orthogonal linear polarizations, enabling the generation of any polarization. We demonstrate this experimentally using dielectric metasurfaces in the terahertz regime. The meta-molecule

is composed of two independent anisotropic dielectric meta-atoms. Each meta-atom provides two effective geometric freedoms. A meta-molecule database that maps the parameter space of geometric degrees of freedom to the parameter space of optical properties is first built and enables complete control over the electromagnetic field as described above. The control over amplitude and phase of orthogonal polarizations can be understood in terms of polarization-dependent interference. Based on that, three proof-of-concept meta-holograms are proposed and demonstrated experimentally, which illustrate polarization-independent, polarization-dependent, and vectorial holography, respectively. The meta-holograms generate the intended intensity, phase and polarization distributions accurately in the imaging plane. Our findings pave the way towards perfect holograms and high-performance metasurface devices with various wavefront manipulation capabilities.

## 2. Results and discussion

### 2.1. Meta-molecule design and the complete meta-molecule database

**Figure 1**a shows a schematic of the designed dielectric meta-molecule made of high-resistance silicon ($\varepsilon$ = 11.9) in a square lattice of period $P$ = 220 μm. The meta-molecule consists of four pillars with a rectangular cross-section and the same height of $h$ = 200 μm. The pillars are respectively placed at the centers of the lattice cell's four quadrants. The two pillars on each diagonal have the same geometry. This leaves four geometric degrees of freedom, which are the four transverse sizes, $D_{x1}$, $D_{y1}$, $D_{x2}$, and $D_{y2}$, as marked in Figure 1a. Except for special cases, such meta-molecules will be anisotropic, with effective main axes along the $x$ and $y$ directions. To get the transmission responses of the meta-molecule, numerical FDTD simulations are applied, in which the four sizes are raster varied in a range from 20 to 100 μm. The working frequency is selected at 1.23 THz, corresponding to a free-space wavelength of 244 μm, which is larger than the period. Thus, the lattice period will not cause any diffraction in air. Figure 1b to 1e illustrate the simulated database of transmission

amplitudes $|t_x|$, $|t_y|$ and phases $\Psi_x$, $\Psi_y$ as a function of the four geometric parameters ($D_{x1}$, $D_{y1}$, $D_{x2}$, $D_{y2}$), respectively, where the subscripts of the transmission parameters represent the corresponding incident polarization states. In order to show these multi-dimensional results, $D_{x1}$ and $D_{y1}$ are represented by the two transverse axes, while $D_{x2}$ and $D_{y2}$ are represented by dots with different size and colour. Thus, each dot in each graph represents a unique meta-molecule with its transmission response represented by its vertical coordinate. Here, the transmission amplitude is defined as the square root of the single intensity transmittance from the silicon substrate across the meta-atoms to the air (see Supplementary Section 1).[33] Though the lattice period and large refractive index of silicon will cause diffraction inside the silicon substrate, it occurs in the opposite propagation direction and thus does not affect the final transmission defined here. Any influence of such diffraction effects has been eliminated by selecting the first transmission of the THz pulse in the time domain, cutting off any later, multiply reflected signals.

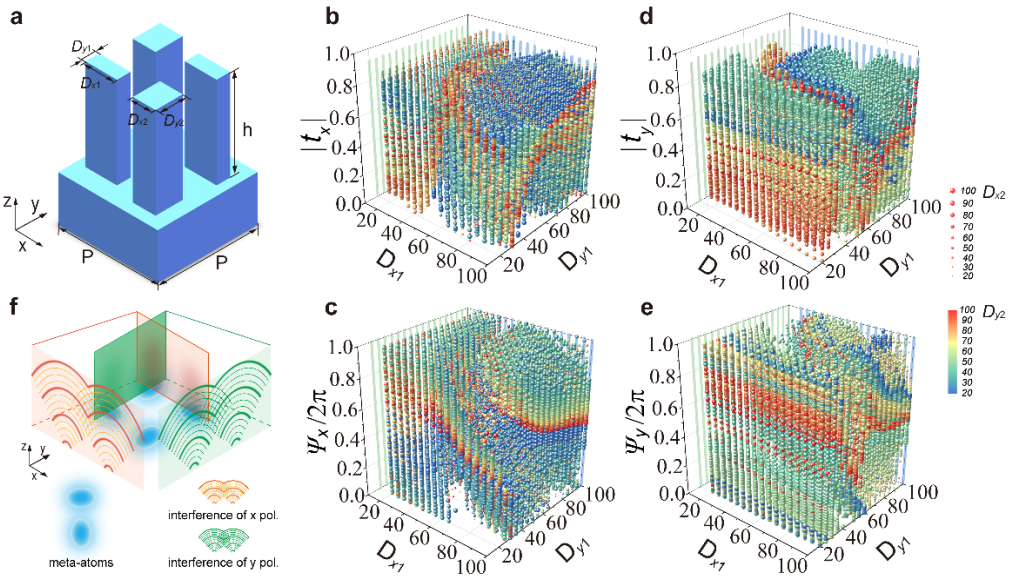


**Figure 1. Meta-molecule design for achieving complete and polarization-dependent control of phase and amplitude. a** Schematic of the dielectric meta-molecule made of silicon, with independent parameters $D_{x1}$, $D_{y1}$, $D_{x2}$, and $D_{y2}$. **b-e** Simulated *x*-polarized **b,c** and *y*-polarized **d,e** transmission amplitudes **b,d** and phases **c,e** for different combinations of $D_{x1}$, $D_{y1}$, $D_{x2}$, $D_{y2}$ in a range from 20 to 100 μm at 1.23 THz under normal incidence conditions, respectively. **f** Schematic of the polarization-dependent interference between two meta-atoms in one meta-molecule in two orthogonal polarization channels.

To show the multi-dimensional data more clearly, the four-dimensional space of optical properties may be presented as a two-dimensional array (representing the phases, $\Psi_x$ and $\Psi_y$) of two-dimensional spaces (representing the amplitudes, $|t_x|$ and $|t_y|$), see **Figure 2**. We divide the phases, $\Psi_x$ and $\Psi_y$, into four $\pi/2$ ranges from 0 to $2\pi$. The entire $\Psi_x$-$|t_x|$-$\Psi_y$-$|t_y|$ space is thus segmented into sixteen two-dimensional sub-plots, each depicting accessible combinations of $|t_x|$ and $|t_y|$ for a different combination of phase ranges for $\Psi_x$ and $\Psi_y$. Each multi-colour scatter represents a meta-molecule whose *x*- and *y*-polarized transmission phases are within the phase ranges of its sub-plot, and whose position within the sub-plot represents its *x*- and *y*-polarized transmission amplitudes. Thus, Figure 2 enables the look-up of meta-molecule geometries (scatter colours) that achieve desired optical properties (scatter position). The orange lines depict the cases of equal *x*- and *y*-polarized transmission coefficients. Scatters that are located on these lines represent meta-molecules possessing polarization-independent responses. It is clearly seen that all sub-plots are filled with scatters, indicating that our database is reasonably complete. Transmission amplitudes reach up to 0.92, substantially more than for a bare silicon-air interface (~0.83), indicating that some meta-molecule designs act as an anti-reflection layer with an effective refractive index in between those of air ($n_{\mathrm{air}} = 1$) and the substrate ($n_{\mathrm{Si}} = 3.45$). Less than unity transmission corresponds to minor blank areas at the top and right sides of all sub-plots in Figure 2. This does not limit the potential functionalities, but it implies minor minimum insertion losses for any metasurface assembled from such meta-molecules. For further evidence of complete control of the transmission amplitudes and phases for *x* and *y* polarization channels see Supplementary Section 2, as well as the dataset that includes the entire simulated meta-molecule database at 1.23 THz.

To understand the essential mechanism of this complete control, one can refer to the polarization-dependent interference effect, as sketched in Figure 1f. Under *j*-polarized illumination, $j = \{x, y\}$, the overall transmitted field of the proposed meta-molecule can be described as the sum of the fields transmitted by the two different pillars $E_j = a_{j1}\exp(i\varphi_{j1}) +$

$a_{j2}\exp(i\varphi_{j2})$ , with $a_{j1}$, $a_{j2}$ and $\varphi_{j1}$, $\varphi_{j2}$ representing the transmission field amplitudes and phases of the two pillars, respectively. Suppose $a_{j1} = a_{j2} = a_j/2$, we have $E_j = a_j\cos[(\varphi_{j1} - \varphi_{j2})/2]\exp[i(\varphi_{j1} + \varphi_{j2})/2]$. Thus, the interference can transform the two phases $\varphi_{j1}$ and $\varphi_{j2}$ to the full range of amplitude $A_j = a_j\cos[(\varphi_{j1} - \varphi_{j2})/2]$ ($\propto |t_j|$) and phase $\Psi = (\varphi_{j1} + \varphi_{j2})/2$, while $\varphi_{j1}$ and $\varphi_{j2}$ can be controlled by ($D_{x1}$, $D_{y1}$) and ($D_{x2}$, $D_{y2}$). However, inevitable coupling among the pillars in the real case makes the interference more complex. Such coupling arises from overlapping leaky fields of the meta-atoms, which makes the overall transmission responses of the meta-molecule deviate from the above interference model, where larger deviations may be expected from stronger coupling. In our design, the silicon pillars can in principle support many possible modes, such as waveguide modes and Mie resonance modes, which can all generate leaky fields. Meanwhile, different meta-atoms may also support different modes. These make it nearly impossible to find a valid universal theory to describe and predict the coupling influence on the overall transmission of all meta-molecules. Detailed information on the influence of the coupling effect can be found in Supplementary Section 3. Thus, we choose to use simulations to build the meta-molecule database in order to obtain more accurate interference responses, which takes coupling within meta-molecules into account and approximates coupling between meta-molecules by considering the response of a periodic structure. Effects due to different geometry of coupled meta-molecules are neglected. As indicated by the analytical model, the simulations confirm that the two pillars in the meta-molecule provide enough interference possibilities to generate a database of unit cells allowing complete control of amplitude and phase of transmitted *x* and *y*-polarized waves.

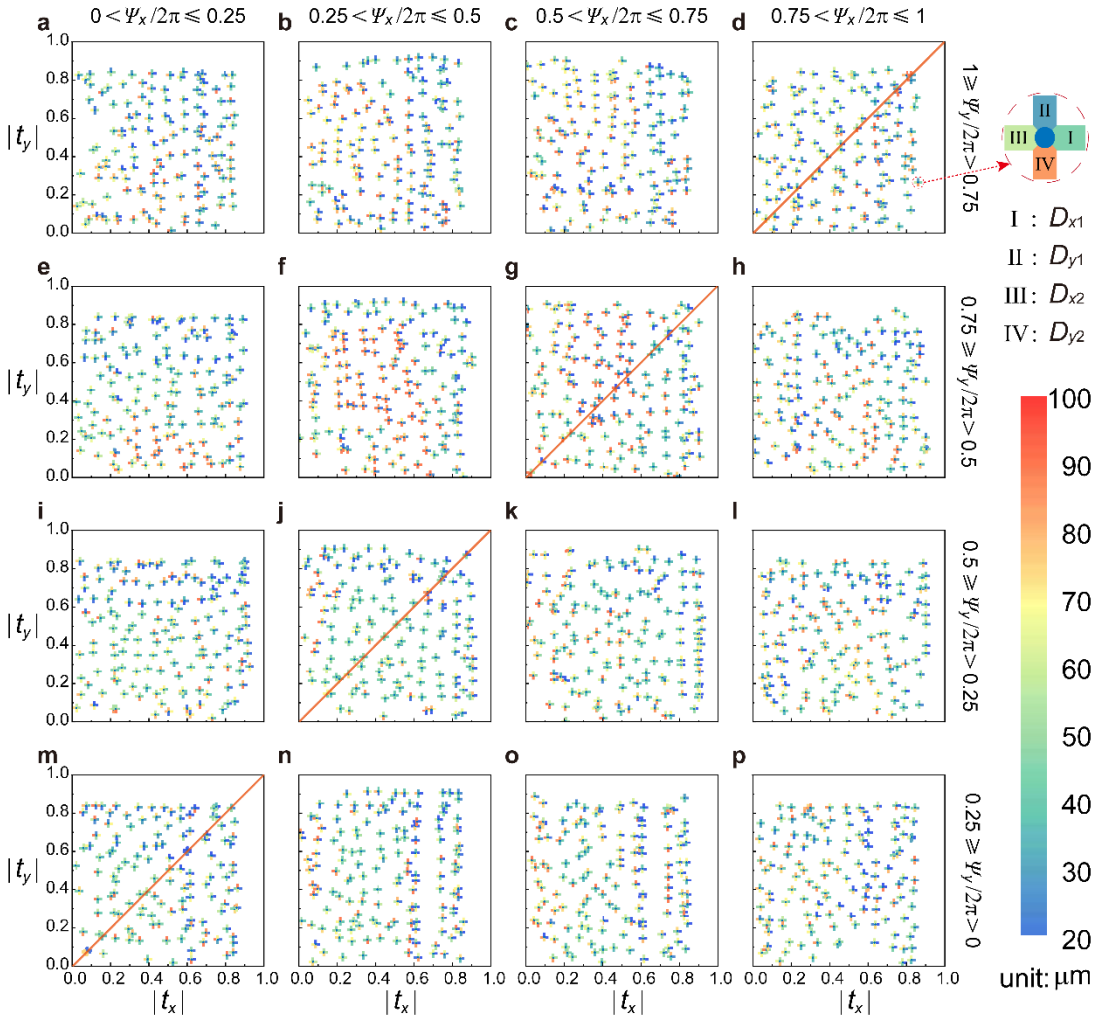


**Figure 2. Completeness of the meta-molecule database. a-p** Distributions of the transmission responses of the meta-molecules in the database (Figure 1b to 1e). Sixteen sub-plots represent π/2 phase ranges of $\Psi_x$ and $\Psi_y$. Each sub-plot shows available combinations of transmission amplitudes $|t_x|$ and $|t_y|$ for the corresponding combination of phase ranges. The inset at the top-right side illustrates the applied multi-colour scatter in a-p with each scatter representing a certain meta-molecule. The scatter is composed of four colour strips marked by I to IV, whose colours respectively correspond to the dimensions $D_{x1}$, $D_{y1}$, $D_{x2}$, and $D_{y2}$ of the meta-molecule it represents. To make the data more readable, only 2.7% of the meta-molecules in the database are included. The orange lines represent polarization-independent transmission responses. When looking up a meta-molecule with desired transmission responses, the desired transmission phases ($\Psi_x$, $\Psi_y$) determine the sub-plot, the desired transmission amplitudes ($|t_x|$, $|t_y|$) determine the position on the sub-plot, and the corresponding meta-molecule geometry ($D_{x1}$, $D_{y1}$, $D_{x2}$, $D_{y2}$) is then read from the colours of the four stripes of the scatter.

### 2.2. Polarization-independent meta-hologram

As a starting point to illustrate our design strategy, a polarization-independent meta-hologram is first designed based on the above meta-molecule database. To implement such control, the meta-molecule should possess certain symmetry to avoid polarization conversion under arbitrarily polarized illumination. There are two kinds of meta-molecules that can satisfy such requirement. One kind has mirror symmetries along the two diagonals, where the two different pillars have square cross-sections with $D_{x1} = D_{y1}$ and $D_{x2} = D_{y2}$. The other kind has a fourfold rotational symmetry (C4), where the two different pillars have rectangular cross-sections with $D_{x1} = D_{y2}$ and $D_{x2} = D_{y1}$. The responses of these two kinds of meta-molecules just locate on the orange lines in Figure 2.

**Figure 3**a schematically illustrates the designed polarization-independent meta-hologram which generates a holographic image of the letter "T". The imaging plane is designed at a distance of 8 mm above the meta-hologram. Figure 3b shows a scanning electron microscope (SEM) image of part of the meta-hologram fabricated using conventional photolithography and deep reactive ion-beam etching (deep RIE, see Methods). The corresponding required amplitude and phase distributions for the meta-hologram are illustrated in Figure 3c and 3d, respectively. They are calculated using the Rayleigh-Sommerfeld diffraction theory by setting a target planar letter "T" of 9.9 mm × 9.9 mm size and with a homogeneous phase distribution as the image source.[19] Then, the meta-hologram is obtained by arranging the meta-molecules with minimum response deviations $(|A_t\exp(i\Psi_t) - |t|\exp(i\Psi)|)_{min}$ from the meta-molecule database to fulfil the required distributions, where $A_t$ and $\Psi_t$ represent the target transmission amplitude and phase at an arbitrary meta-molecule position, and $|t|$ and $\Psi$ represent the transmission amplitudes and phases of the meta-molecules that fulfil the above-mentioned symmetries. The final designed meta-hologram is composed of 45 × 45 meta-molecules with an overall size of 9.9 mm × 9.9 mm, where the responses of all selected meta-molecules match the target responses very well (see Supplementary Section 4).

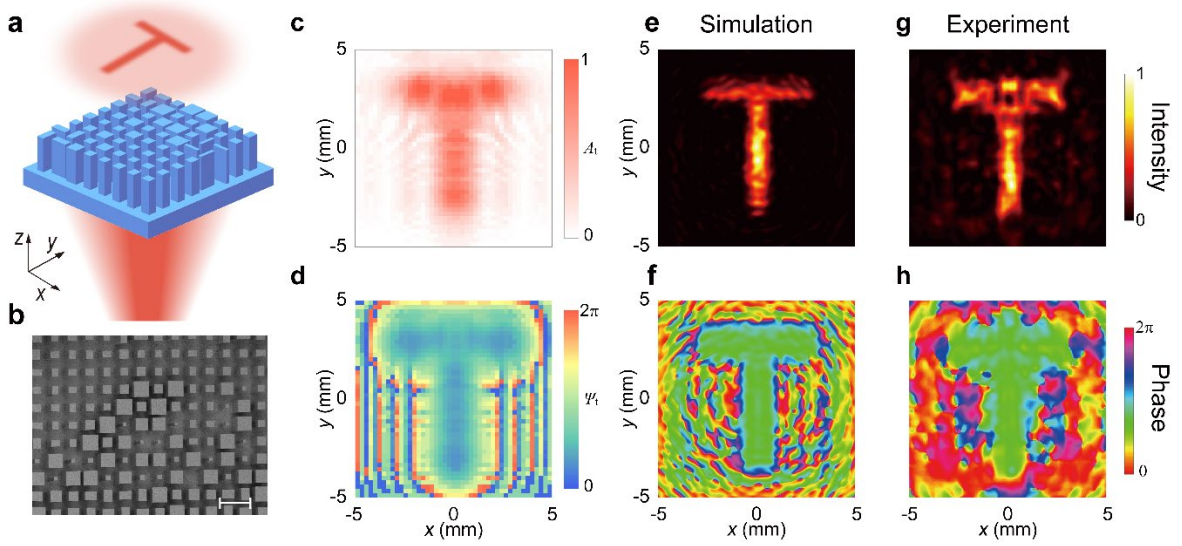


**Figure 3. Polarization-independent meta-hologram. a** Schematic illustrating the generation of the same image for illumination of the meta-hologram with any polarization. **b** SEM image of part of the fabricated meta-hologram. Scale bar: 200 μm. **c,d** Calculated amplitude ($A_t$) **c** and phase ($\Psi_t$) **d** distributions of the meta-hologram for generating a letter "T". **e,f** Simulated intensity **e** and phase **f** distributions of the holographic image generated 8 mm above the meta-hologram under *x*-polarized illumination at 1.23 THz. **g,h** Corresponding measured intensity **g** and phase **h** distributions.

Figure 3e and 3f shows the simulated intensity and phase distributions of the holographic image generated 8 mm above the meta-hologram at 1.23 THz under *x*-polarized illumination, respectively. A clear letter "T" is obtained, where the gradual intensity reduction outside the central area (Figure 3e) is attributed to the Gaussian beam illumination in the simulation. More importantly, the phase distribution is also well reconstructed, as indicated by the homogeneous phase distribution in the "T" area in Figure 3f, which shows an even higher imaging quality with sharp edges. Such simultaneous intensity and phase imaging capacity stems from the simultaneous control over phase and amplitude and cannot be obtained with phase control alone (see Supplementary Section 5). Figure 3g and 3h illustrate the measured intensity and phase distributions of the holographic image at the designed imaging distance using our home-build fiber-based near-field scanning terahertz microscope system (see Methods). It can be seen that the letter "T" is clearly obtained in both the measured intensity and phase distributions, which coincide well with the corresponding simulations in Figure 3e

and 3f. Similar results were also obtained under illumination with different polarizations (see Supplementary Section 6), demonstrating the polarization-independent wavefront control capability of our method.

### 2.3. Polarization-dependent meta-hologram

The above results have demonstrated our design strategy in achieving polarization-independent phase and amplitude control, which relies on only a small subset of our meta-molecule database. To further demonstrate its capabilities, a polarization-dependent meta-hologram which generates different holographic images, of the letters "A" and "P", under *x*- and *y*-polarized illumination is designed, as illustrated by **Figure 4**a. Figure 4b shows an SEM image of part of the fabricated meta-hologram. Similarly, the required amplitude and phase distributions of the meta-hologram in the two orthogonal polarization channels are calculated separately with the target 9.9 mm × 9.9 mm images (letter "A" and letter "P") also placed at a distance of 8 mm above the meta-hologram. Both the target images have an initially homogeneous phase distribution. The corresponding results are shown by Figure 4c to 4f, respectively. In designing the meta-hologram, the meta-molecule at each position should simultaneously satisfy the amplitude and phase responses at the same position in Figure 4c and 4d for *x*-polarized illumination, and in Figure 4e and 4f for *y*-polarized illumination. To fulfil this requirement, each meta-molecule in the meta-hologram is selected by choosing the one that can provide the minimum response deviation $(|A_{tx}\exp(i\Psi_{tx}) - |t_x|\exp(i\Psi_x)| + |A_{ty}\exp(i\Psi_{ty}) - |t_y|\exp(i\Psi_y)|)_{min}$ from the meta-molecule database in Figure 1b to 1e. Here, $A_{tx}$, $A_{ty}$ and $\Psi_{tx}$, $\Psi_{ty}$ represent the target transmission amplitudes and phases in the *x*- and *y*-polarization channels at an arbitrary meta-molecule position, $|t_x|$, $|t_y|$ and $\Psi_x$, $\Psi_y$ represent the transmission amplitudes and phases of all the meta-molecules in the meta-molecule database. The final meta-hologram is also composed of 45 × 45 meta-molecules with an overall size of

9.9 mm × 9.9 mm, where the responses of all selected meta-molecules match the target responses very well (see Supplementary Section 4).

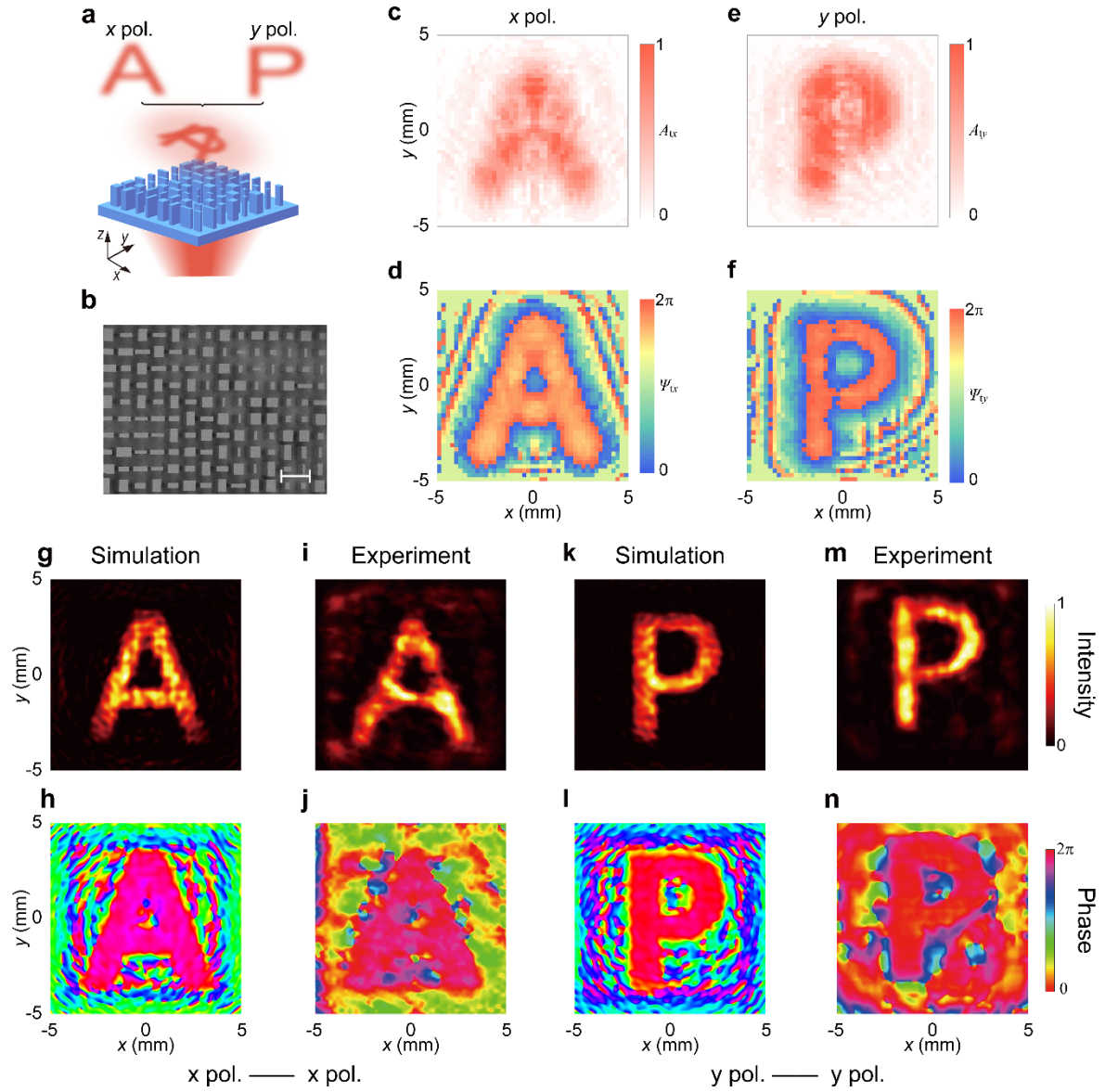


**Figure 4. Polarization-dependent meta-hologram. a** Schematic illustrating the generation of independent images for *x*-polarized and *y*-polarized illumination of the meta-hologram. **b** SEM image of part of the fabricated meta-hologram. Scale bar: 200 μm. **c-f** Calculated *x*-polarized **c,d** and *y*-polarized **e,f** amplitude ($A_{tx}$, $A_{ty}$) **c,e** and phase ($\Psi_{tx}$, $\Psi_{ty}$) **d,f** distributions of the meta-hologram. **g-j** Simulated **g,h** and measured **i,j** intensity **g,i** and phase **h,j** distributions of the holographic image generated 8 mm above the meta-hologram under *x*-polarized illumination. **k-n** Simulated **k,l** and measured **m,n** intensity **k,m** and phase **l,n** distributions of the holographic image generated 8 mm above the meta-hologram under *y*-polarized illumination.

Figure 4g,4h and 4k,4l illustrate the simulated intensity and phase distributions of the holographic images generated 8 mm above the meta-hologram at 1.23 THz under *x*- and *y*-

polarized illumination, respectively. Clear letters “A” and letters “P” are obtained in both the intensity and phase distributions matching the design. As before, due to the intensity distribution of the Gaussian beam, the center part of the image is brighter. Figure 4i,4j and 4m,4n illustrate the corresponding measured results (see Methods), which agree well with the simulations. Such results demonstrate the capability of our method to provide complete control over phase and amplitude independently for two orthogonal linear polarization states.

### 2.4. Vectorial meta-hologram

The above meta-holograms only make separate use of the *x*- and *y*-polarization channels. In this section, we show that our design strategy allows even more complex wavefront control based on exploiting both orthogonal polarization channels simultaneously. To demonstrate this versatile capability, a vectorial meta-hologram is designed, as illustrated in **Figure 5**a. The target image is a vectorial ring, where the intensity changes as $I \propto \cos(\theta - \pi/4)$ and the polarization orientation changes as $\theta + \pi/2$ with $\theta$ being the azimuthal angle. The intensity and polarization of the vectorial ring are homogenous along the radial direction. Here, the holographic image is also designed to be 8 mm above the meta-hologram and the size is 5 mm × 5 mm. Figure 5b shows an SEM image of part of the fabricated meta-hologram. Owing to the vectorial nature of the image, it can be first decomposed into two separate *x*- and *y*-polarized images. By using the same design method as for the above polarization-dependent meta-hologram, the required phase and amplitude distributions of the meta-hologram in the two orthogonal polarization channels are calculated, as respectively illustrated in Figure 5c and 5d for *x*-polarized illumination and Figure 5e and 5f for *y*-polarized illumination. According to them, the meta-hologram is designed by carefully selecting and arranging the meta-molecules. The overall size of the final meta-hologram is the same as for the above meta-holograms, where the responses of all the selected meta-molecules match the target responses very well (see Supplementary Section 4). Since no phase difference and relative

amplitude scaling is introduced in the meta-hologram design, 45° linearly polarized light is required to reconstruct the vectorial image. Figure 5g and 5h show the simulated and measured intensity distributions of the holographic image generated 8 mm above the meta-hologram at 1.23 THz under 45°-polarized illumination. Here, the intensity at each point is the sum of the squares of the corresponding absolute *x*- and *y*-polarized electric fields. The intended azimuthal intensity distribution is clearly obtained with intensity maxima and minima located at around $\theta = 45°$, 225° and 135°, 315°, respectively. The simulated and measured polarization states along a central circle of the generated rings are marked in Figure 5g and 5h. A clear azimuthal polarization distribution is observed. Besides fabrication imperfections, small deviations of the polarization distribution relative to target one is also related to some measurement uncertainty arising from the polarizer rotation operations (see Methods). Even so, our results have unambiguously demonstrated the vectorial wavefront control capability of our method.

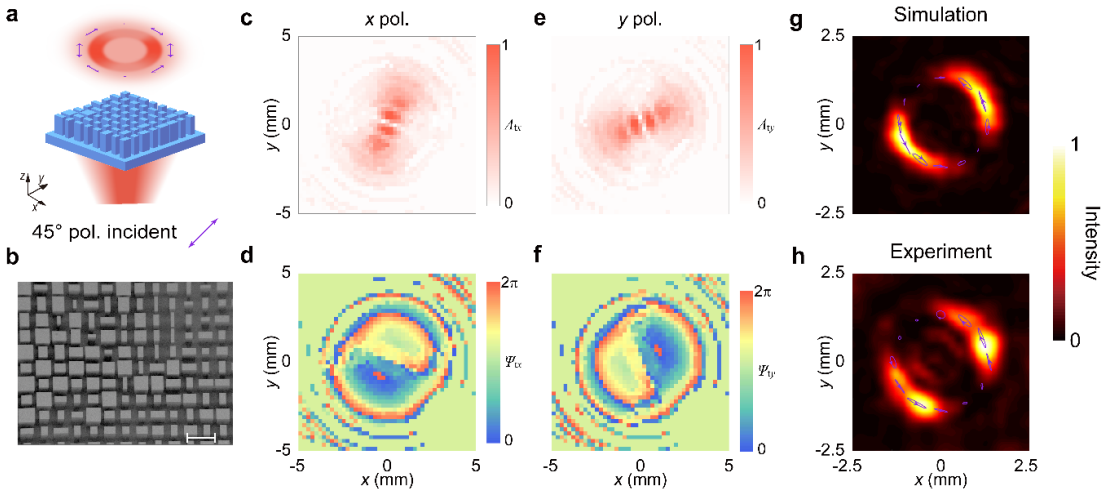


**Figure 5. Vectorial meta-hologram. a** Schematic illustrating the generation of an azimuthally polarized vector beam by the vectorial meta-hologram. **d** SEM image of part of the fabricated meta-hologram. Scale bar: 200 μm. **c-f** Calculated *x*-polarized **c,d** and *y*-polarized **e,f** amplitude ($A_{tx}$, $A_{ty}$) **c,e** and phase ($\Psi_{tx}$, $\Psi_{ty}$) **d,f** distributions of the meta-hologram. **g,h** Simulated **g** and measured **h** intensity distributions of the holographic image generated 8 mm above the meta-hologram under 45°-polarized illumination. The inset arrows along a ring depict the corresponding polarization distribution.

### 2.5. Discussion

In building the meta-molecule database, only the transmission at the meta-molecule interface is considered. However, in real cases, there is a flat and bare air-silicon interface at the other side of the silicon substrate, which will bring about 30% reflection loss. Though it does not affect the imaging quality, it will reduce the working efficiency. This can be addressed by adding an antireflection film[45] or metasurface[33,46] on this interface. Here, an antireflection silicon metasurface is further proposed, which is a periodic array of square-shaped silicon pillars with side lengths $D_x = D_y = 36.9$ μm, height $h = 32.3$ μm and periods $P_x = P_y = 50$ μm. The isotropic meta-atom design guarantees a polarization-independent response, and the simulation indicates almost 100% transmittance at 1.23 THz. Detailed information on this antireflection metasurface can be found in Supplementary Section 7 and Figure S7. Such a metasurface can be conveniently fabricated by the same technique as the proposed meta-holograms, and can also be used to reduce or even eliminate multiple reflections within the substrate.

The working bandwidth is an important performance parameter of an optic device. However, the interference-based working principle of our meta-molecules limits their bandwidth owing to the different dispersion responses of the constituent meta-atoms. Thus, the perturbations of transmission amplitude and phase resulting from a change of the working frequency will be different for different meta-molecules and also depend on the coupling between the contained meta-atoms. Therefore, the bandwidth will vary somewhat from meta-device to meta-device. To characterize the working bandwidth of our meta-holograms, the overall holographic responses of the meta-holograms at different frequencies around the working frequency are evaluated (see Supplementary Section 8). Based on this method, the effective working bandwidths of the polarization-independent, polarization-dependent, and vectorial meta-holograms are about 0.2 THz, 0.15 THz (0.15 THz for *x*-polarized illumination

and 0.25 THz for *y*-polarized illumination), and 0.15 THz, respectively. Beyond these frequency ranges, the imaging quality drops quickly.

## 3. Conclusion

We have proposed and demonstrated a generic design strategy for achieving complete control of phase, amplitude and polarization. By introducing multiple meta-atoms into the meta-molecule design, we obtain four geometric degrees of freedom that are sufficient to achieve independent control over amplitude and phase for orthogonal linear polarizations based on polarization-dependent interference. We demonstrate that this is sufficient to access the entire parameter space of amplitudes and phases, apart from minor insertion losses. Our design can be fabricated easily as it only requires single-layer structures. To show the capabilities of our method, three meta-holograms have been designed and experimentally characterized. Good polarization-independent, polarization-dependent, and vectorial imaging performances are demonstrated numerically and experimentally. The simultaneous intensity and phase imaging capability based on simultaneous phase and amplitude control allows the design of phase images and phase difference images between the *x*- and *y*-polarized outputs. While the demonstrated vectorial hologram exhibited a linear polarization distribution, we note that our method allows for arbitrary polarization distributions. As complete and independent control of amplitude and phase of orthogonal linear polarization states (*x* and *y*) enables complete polarization control, our method allows the full recovery to the target field and is able to realize arbitrary vector holography, in principle for any known incident polarization that contains non-negligible *x* and *y* components (see Supplementary Section 9). Moreover, other functionalities like multi-direction wavefront manipulation, 3D vectorial holography, complex structured light generation, and so on, could also be realized with the current method. Such capability may find broad applications in multi-channel communications, light field regulation, and image encryption, etc. We believe our design strategy can serve as a promising

route towards versatile novel and multi-functional optical devices. Though the method is demonstrated in the linear polarization basis, it could in principle be extended to the circular polarization basis for achieving spin-dependent functionalities.

## 4. Experimental Section

*Sample fabrication*: The dielectric metasurfaces were fabricated using conventional photolithography and etching. Firstly, a chromium layer of about 10-nm thickness was sputtered on the 1-mm-thick high-resistivity double-side-polished silicon wafer. Secondly, a layer of 7-μm-thick AZ2070 photoresist was spin-coated on top of the wafer. Next, the photoresist was patterned by conventional photolithography with a photo mask and developed. Then, the chromium areas that were not protected by the photoresist were removed by acid eroding. After that, deep reactive ion etching was employed to etch the unwanted silicon areas to a depth of 200 μm, where the remaining photoresist and chromium served as a hard mask. At last, the dielectric metasurfaces were finalized by separately cleaning the residual photoresist and chromium with acetone and acid.

*Experimental Characterization*: All the meta-holograms were characterized by a homo-made fiber-based near-field scanning terahertz microscopy (FNSTM) system,[47,48] as illustrated in Supplementary Section 10. The terahertz emitter was a commercially available fiber-based terahertz photoconductive antenna (@1550 nm, Menlon Inc.), which was set to generate *x*-polarized terahertz waves. Then, the terahertz waves were collected and collimated by a terahertz lens with a focus length of 50 mm. Before illuminating them onto the meta-holograms, a linear polarizer (P1) was inserted to initialize the incident polarization. After passing through the meta-holograms, another linear polarizer (P2) was inserted to extract the desired output polarization components. At last, the terahertz fields were detected by a commercially available photoconductive-antenna-based terahertz near-field probe with a

resolution up to 20 μm (Teraspike), which was placed at 8 mm distance above the meta-holograms and set to only detect the *x*-polarized terahertz waves. The terahertz field distributions were measured by raster scanning the positions of the meta-holograms using an electrically controlled translation stage, while the positions of the incident terahertz wave and the terahertz probe were held. The obtained terahertz fields were initially time-domain signals. By taking Fourier transform of each signal into the frequency domain and then extracting the intensity and phase values at the designed frequency, the intensity and phase distributions of the holographic images were obtained.

For measuring the polarization-independent meta-hologram, both P1 and P2 were set to only allow the x-polarized transmission. To measure the polarization-independent feature in Supplementary Section 6, we rotated the meta-hologram by 0°, 45°, 90°, and 135° instead of varying the incident and detected polarization states to achieve the desired incident polarizations. For measuring the polarization-dependent meta-hologram, the polarization-dependent responses were measured using a similar method through rotating the meta-hologram by either 0° or 90°. In both cases, the whole applied scanning ranges in the x and y directions were large enough to cover the effective holographic images. The scanning step was 0.2 mm. For measuring the vectorial meta-hologram, the incident 45°-polarized terahertz wave was realized by rotating P1 by 45°. To allow the polarization analysis of the generated holographic image, P2 was rotated by either 45° or −45° to allow extraction of the corresponding field distributions of the 45° and −45° polarization components, since these two components contribute the same polarization projection to the *x*-polarized terahertz probe. Then, the polarization distribution of the image generated by the vectorial meta-hologram was obtained by synthesizing the two field distributions. The scanning area in this case was 5 mm × 5 mm with a step of 0.2 mm.

**Supporting Information**

Supporting Information is available from the Wiley Online Library or from the author.

**Acknowledgements**
This work is supported by the National Key Research and Development Program of China (Grant No. 2017YFA0701004); the National Natural Science Foundation of China (Grant Nos. 62075158, 11974259, 61735012, 62005193, 62025504, 61875150, 61935015); the Tianjin Municipal Fund for Distinguished Young Scholars (18JCJQJC45600); the UK's Engineering and Physical Sciences Research Council (Grant Nos. EP/M009122/1 and EP/T02643X/1); H2020 ERC Consolidator Grant (648783).

**Data Availability Statement**
The data that support the findings of this study are openly available from the University of Southampton ePrints research repository at https://doi.org/10.5258/SOTON/D1945.

Received:
Revised:
Published online:

References

[1] H.-T. Chen, A. J Taylor, N. Yu, *Rep. Prog. Phys.* **2016**, 79, 07640.

[2] S. M. Kamali, E. Arbabi, A. Arbabi, A. Faraon, *Nanophotonics* **2018**, 7, 1041.

[3] S. Sun, Q. He, J. Hao, S. Xiao, L. Zhou, *Adv. Opt. Photonics* **2019**, 11, 380.

[4] N. Yu, P. Genevet, M. A. Kats, F. Aieta, J.-P. Tetienne, F. Capasso, Z. Gaburro, *Science* **2011**, 334, 333.

[5] X. Zhang, Z. Tian, W. Yue, J. Gu, S. Zhang, J. Han, W. Zhang, *Adv. Mater.* **2013**, 25, 4567.

[6] D. Sell, J. Yang, S. Doshay, R. Yang, J. A. Fan, *Nano Lett.* **2017**, 17, 3752.

[7] T. Cai, S. Tang, B. Zheng, G. Wang, W. Ji, C. Qian, Z. Wang, E. Li, H. Chen, *Adv. Photonics* **2020**, 3, 016001.

[8] M. Khorasaninejad, W. T. Chen, R. C. Devlin, J. Oh, A. Y. Zhu, F. Capasso, *Science* **2016**, 352, 1190.

[9] W. T. Chen, A. Y. Zhu, V. Sanjeev, M. Khorasaninejad, Z. Shi, E. Lee, F. Capasso, *Nat. Nanotechnol.* **2018**, 13, 220.

[10] W. Liu, Z. Li, H. Cheng, C. Tang, J. Li, S. Zhang, S. Chen, J. Tian, *Adv. Mater.* **2018**, 30, 1706368.

[11] Q. Fan, W. Zhu, Y. Liang, P. Huo, C. Zhang, A. Agrawal, K. Huang, X. Luo, Y. Lu, C. Qiu, H. J. Lezec, T. Xu, *Nano Lett.* **2019**, 19, 1158.

[12] J. Wen, L. Chen, X. Chen, S. Kanwal, L. Zhang, S. Zhuang, D. Zhang, D. Lei, *Laser Photonics Rev.* **2021**, 15, 2000487.

[13] M. Liu, P. Huo, W. Zhu, C. Zhang, S. Zhang, M. Song, S. Zhang, Q. Zhou, L. Chen, H. J. Lezec, A. Agrawal, Y. Lu, T. Xu, *Nat. Commun.* **2021**, 12, 2230.

[14] G. Zheng, H. Mühlenbernd, M. Kenney, G. Li, T. Zentgraf, S. Zhang, *Nat. Nanotechnol.* **2015**, 10, 308.

[15] M. Khorasaninejad, A. Ambrosio, P. Kanhaiya, F. Capasso, *Sci. Adv.* **2016**, 2, e1501258.

[16] L. Li, T. J. Cui, W. Ji, S. Liu, J. Ding, X. Wan, Y. B. Li, M. Jiang, C.-W. Qiu, S. Zhang, *Nat. Commun.* **2017**, 8, 197.

[17] D. Wen, J. J. Cadusch, J. Meng, K. B. Crozier, *Adv. Photonics* **2021**, 3, 024001.

[18] S. Chen, Z. Li, W. Liu, H. Cheng, J. Tian, *Adv. Mater.* **2019**, 31, 1802458.

[19] Q. Wang, X. Zhang, Y. Xu, J. Gu, Y. Li, Z. Tian, R. Singh, S. Zhang, J. Han, W. Zhang, *Sci. Rep.* **2016**, 6, 32867.

[20] C. Overvig, S. Shrestha, S. C. Malek, M. Lu, A. Stein, C. Zheng, N. Yu, *Light: Sci. Appl.* **2019**, 8, 92.

[21] H. Ren, X. Fang, J. Jang, J. Bürger, J. Rho, S. A. Maier, *Nat. Nanotechnol.* **2020**, 15, 948.

[22] A. Arbabi, Y. Horie, M. Bagheri, A. Faraon, *Nat. Nanotechnol.* **2015**, 10, 937.

[23] D. Wang, F. Liu, T. Liu, S. Sun, Q. He, L. Zhou, *Light: Sci. Appl.* **2021**, 10, 67.

[24] X. Zhang, S. Yang, W. Yue, Q. Xu, C. Tian, X. Zhang, E. Plum, S. Zhang, J. Han, W. Zhang, *Optica* **2019**, 6, 1190.

[25] I. Kuznetsov, A. E. Miroshnichenko, M. L. Brongersma, Y. S. Kivshar, B. Luk'yanchuk, *Science* **2016**, 354, aag2472.

[26] P. Genevet, F. Capasso, F. Aieta, M. Khorasaninejad, R. Devlin, *Optica* **2017**, 4, 139.

[27] N. Yu, F. Capasso, *Nat. Mater.* **2014**, 13, 139.

[28] S. Sun, Q. He, S. Xiao, Q. Xu, X. Li, L. Zhou, *Nat. Mater.* **2012**, 11, 426.

[29] H. Zhang, X. Zhang, Q. Xu, Q. Wang, Y. Xu, M. Wei, Y. Li, J. Gu, Z. Tian, C. Ouyang, X. Zhang, C. Hu, J. Han, W. Zhang, *Photonics Res.* **2017**, 6, 24.

[30] L. Huang, X. Chen, H. Mühlenbernd, G. Li, B. Bai, Q. Tan, G. Jin, T. Zentgraf, S. Zhang, *Nano Lett.* **2012**, 12, 5750.

[31] L. Liu, X. Zhang, M. Kenney, X. Su, N. Xu, C. Ouyang, Y. Shi, J. Han, W. Zhang, S. Zhang, *Adv. Mater.* **2014**, 26, 5031.

[32] Q. Wang, Q. Xu, X. Zhang, C. Tian, Y. Xu, J. Gu, Z. Tian, C. Ouyang, X. Zhang, J. Han, W. Zhang, *ACS Photonics* **2017**, 5, 599.

[33] H. Zhang, X. Zhang, Q. Xu, C. Tian, Q. Wang, Y. Xu, Y. Li, J. Gu, Z. Tian, C. Ouyang, X. Zhang, C. Hu, J. Han, W. Zhang, *Adv. Opt. Mater.* **2018**, 6, 1700773.

[34] F. Ding, R. Deshpande, S. I. Bozhevolnyi, *Light: Sci. Appl.* **2018**, 7, 17178.

[35] E. Arbabi, A. Arbabi, S. M. Kamali, Y. Horie, A. Faraon, *Optica* **2016**, 3, 628.

[36] Q. Wang, E. Plum, Q. Yang, X. Zhang, Q. Xu, Y. Xu, J. Han, W. Zhang, *Light: Sci. Appl.* **2018**, 7, 25.

[37] S. Wang, Z.-L. Deng, Y. Wang, Q. Zhou, X. Wang, Y. Cao, B.-O. Guan, S. Xiao, X. Li, *Light: Sci. Appl.* **2021**, 10, 24.

[38] Y. Bao, Y. Yu, H. Xu, C. Guo, J. Li, S. Sun, Z.-K. Zhou, C.-W. Qiu, X.-H. Wang, *Light: Sci. Appl.* **2019**, 8, 95.

[39] Q. Fan, M. Liu, C. Zhang, W. Zhu, Y. Wang, P. Lin, F. Yan, L. Chen, H. J. Lezec, Y. Lu, A. Agrawal, T. Xu, *Phys. Rev. Lett.* **2020**, 125, 267402.

[40] Y. Bao, J. Ni, C.-W. Qiu, *Adv. Mater.* **2020**, 32, 1905659.

[41] J. Li, P. Yu, S. Zhang, N. Liu, *Nat. Commun.* **2020**, 11, 3574.

[42] Y. Zhou, I. I. Kravchenko, H. Wang, H. Zheng, G. Gu, J. Valentine, *Light: Sci. Appl.* **2019**, 8, 80.

[43] Z.-L. Deng, M. Jin, X. Ye, S. Wang, T. Shi, J. Deng, N. Mao, Y. Cao, B.-O. Guan, A. Alù, G. Li, X. Li, *Adv. Funct. Mater.* **2020**, 30, 1910610.

[44] M. Liu, W. Zhu, P. Huo, L. Feng, M. Song, C. Zhang, L. Chen, H. J. Lezec, Y. Lu, A. Agrawal, T. Xu, *Light: Sci. Appl.* **2021**, 10, 107.

[45] A. J. Gatesman, J. Waldman, M. Ji, C. Musante, S. Yngvesson, IEEE Microw. Guided Wave Lett. **2000**, 10, 264.

[46] A. Cordaro, J. Groep, S. Raza, E. F. Pecora, F. Priolo, M. L. Brongersma, *ACS Photonics* **2019**, 6, 453.

[47] Q. Wang, X. Zhang, Y. Xu, Z. Tian, J. Gu, W. Yue, S. Zhang, J. Han, W. Zhang, *Adv. Opt. Mater.* **2015**, 3, 779.

[48] Y. Xu, H. Zhang, Q. Li, X. Zhang, Q. Xu, W. Zhang, C. Hu, X. Zhang, J. Han, W. Zhang, *Nanophotonics* **2020**, 9, 3393.

[dataset] T. Wu, X. Zhang, Q. Xu, E. Plum, K. Chen, Y. Xu, Y. Lu, H. Zhang, Z. Zhang, X. Chen, G. Ren, L. Niu, Z. Tian, J. Han, W. Zhang, 2021, Dataset for Dielectric metasurfaces for complete control of phase, amplitude and polarization, University of Southampton ePrints research repository, https://doi.org/10.5258/SOTON/D1945.